69% hydrogenation (sample 11) into two distinct maxima which shift to higher temperatures as the ethylene content increases. These are listed as T_1 and T_2 in Table II. In sample 11, T_2 is found in the temperature range normally associated with the β relaxation in polyethylene, but this moves rapidly into a position (sample 15) near where the α relaxation is detected in polyethylene. There is now no distinct baseline shift, characteristic of T_g, in the DSC thermogram for sample 11, but the melting endotherm is quite pronounced and becomes increasingly so through to sample 15. The β relaxation is usually thought to be a consequence of a relaxation involving branch points in low-density polyethylene. The original *cis*-polybutadiene sample had less than 3% 1,2-addition units present so that the contribution from branch points should be similar to low-density polyethylene, but because the branches are shorter it would appear more likely that the T_2 peaks arise from relaxation processes involving the amorphous regions of small imperfect crystallites.

The spectrum of sample 15 is similar to that of a high-density polyethylene sample in which an α and an α' peak are resolved. Both are attributed to molecular motion believed to originate in the crystalline regions.[26]

Conclusions

On the basis of the evidence presented here it is concluded that the glass transition temperature of completely amorphous polyethylene would lie in the region 190–200 K and that the γ relaxation, while associated with amorphous regions in the polymer, is not the major glass transition temperature. As the rate of crystallization of polyethylene is much too rapid to allow direct measurements on a stable amorphous sample, the significance of T_g in polyethylene remains somewhat academic.

References and Notes

(1) F. C. Stehling and L. Mandelkern, *Macromolecules*, **3**, 242 (1970).
(2) R. F. Boyer, *Macromolecules*, **6**, 285 (1973).
(3) E. W. Fischer and F. Kloos, *J. Polym. Sci., Part B*, **8**, 685 (1970).
(4) C. L. Beatty and F. E. Karasz, *Bull. Am. Phys. Soc.* **16**, Ac-12 (1971).
(5) P. J. Hendra, H. P. Jobic, and K. Holland-Moritz, *J. Polym. Sci., Part B*, **13**, 365 (1975).
(6) R. F. Boyer, *J. Macromol. Sci., Phys.*, **8**, 503 (1973).
(7) J. J. Maurer, *Rubber Chem. Technol.*, **38**, 979 (1965).
(8) M. Gordon and J. S. Taylor, *J. Appl. Chem.*, **2**, 493 (1952).
(9) R.-H. Illers, *Kolloid Z. Z. Polym.*, **190**, 16 (1963).
(10) E. G. Kontos and W. P. Slichter, *J. Polym. Sci.*, **61**, 61 (1962).
(11) I. Baldi and R. Zannetti, *Mater. Plast. Elastomeri*, **31**, 1309 (1965).
(12) L. E. Nielsen, *J. Polym. Sci.*, **42**, 357 (1960).
(13) C. A. F. Tuijnman, *J. Polym. Sci., Part C*, **16**, 2379 (1967).
(14) M. Takeda and R. Endo, *Rep. Prog. Polym. Phys. Jpn.*, **6**, 37 (1963).
(15) J. L. Binder, *Appl. Spectrosc.*, **28**, 17 (1969).
(16) L. A. Mango and R. W. Lenz, *Makromol. Chem.*, **163**, 13 (1973).
(17) A. F. Lewis and J. K. Gillham, *J. Appl. Polym. Sci.*, **6**, 422 (1962).
(18) J. K. Gillham, *Crit. Rev. Macromol. Sci.*, **1**, 83 (1972).
(19) J. M. Barton, *J. Polym. Sci., Part C*, **30**, 573 (1970).
(20) D. Lath, personal communication.
(21) (a) J. L. Zakin, H. C. Hershey, and R. Simha, *J. Appl. Polym. Sci.*, **10**, 1455 (1966); (b) S. Lee and R. Simha, *Macromolecules*, **7**, 909 (1974).
(22) R. K. Jain, R. N. Gupta, and V. S. Nanda, *J. Macromol. Sci., Phys.*, **11**, 411 (1975).
(23) D. E. Kline, J. A. Sauer, and A. E. Woodward, *J. Polym. Sci.*, **22**, 455 (1955).
(24) R. Sanui, W. J. MacKnight, and R. W. Lenz, *Macromolecules*, **7**, 101 (1974).
(25) T. R. Earnest, Jr., and W. J. MacKnight, *Macromolecules*, **10**, 206 (1977).
(26) N. G. McCrum, B. E. Reid, and G. Williams, "Anelastic and Dielectric Effects in Polymeric Solids", Wiley, New York, N.Y., 1967.

Neutron Scattering Studies on the Molecular Trajectory in Polyethylene Crystallized from Solution and Melt†

D. M. Sadler* and A. Keller

H. H. Wills Physics Laboratory, University of Bristol, Royal Fort, Bristol BS8 1TL, England.

Received May 10, 1977

ABSTRACT: A comparative survey was carried out on the trajectory of polyethylene chains within their own crystal environment in the case of solution- and melt-crystallized samples by means of low-angle neutron scattering using the isotope miture method. The issue of prime concern was the manner of fold re-entry as assessed by the arrangement of the straight segments. However, to ensure molecular dispersion of the labeled minority species total scattering mass and radius of gyration were also studied to a lesser extent, the full range of measurements extending over the rather wide angular range from 1400 to 16 Å equivalent Bragg spacing. The principal result was that in solution-grown crystals the chains form sheets consistent with adjacent fold re-entry, confirming earlier claims,[15] in sharp contrast to samples crystallized from a cooling melt where the effectively random arrangements of stems imply random fold re-entry. It is believed these two cases are extremes of a general behavior pattern. Scattering effects in the lowest angular range were interpretable in terms of enrichment of the labeled species along the periphery of large-scale morphological units, as opposed to molecular associations, where very low levels of enrichment sufficed to account for the observed effects. How far effects of this kind permit or limit the interpretation of neutron diffraction data in wider angular ranges has been evaluated and discussed. Other discussions are concerned with a number of effects observed relating to variations in molecular weight, crystallization temperature, concentration of the labeled species, and the significance of the findings in general.

General Background

The basic issue underlying this paper is the nature of chain folding in crystalline polyethylene: specifically what is the manner of re-entry and how this is affected by crystallization conditions, in particular when crystallization from solution and melts are compared. These have been long-standing problems which can now be approached from a new angle thanks to the recently introduced method of neutron scattering from isotopically tagged molecules. Deuterated molecules are mixed in small concentrations with the protonated version of the same species, or vice versa, when, owing to the largely differing scattering amplitudes of H and D, the mi-

† Dedicated to the 80th birthday of Professor Maurice L. Huggins.

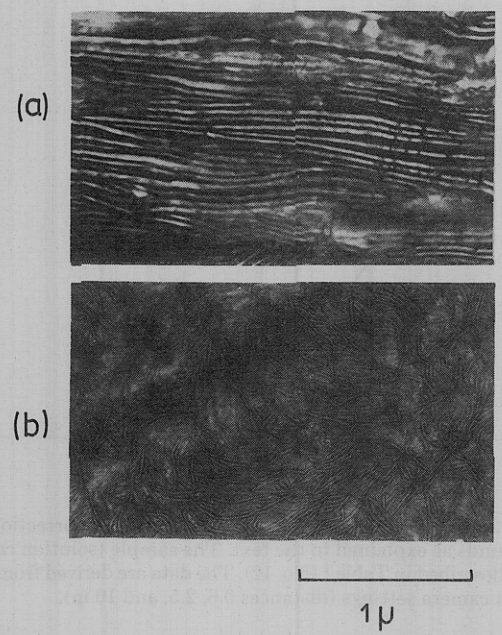

Figure 1. Electron micrographs of sections of melt-grown polyethylene crystals by a recently developed staining technique[7,8] by courtesy of D. T. Grubb of this laboratory: (a) isothermal growth at 127 °C; (b) quenched material (this blend was the same as used for sample 18 in Table I). The micrographs illustrate clearly the existence of lamellae for two very different conditions of crystallization. However, their thicknesses and arrangements differ in (a) and (b).

nority component can be analyzed by neutron scattering at low angles as regards shape, mass, and internal structure. This method has already been extensively applied to amorphous polymers and solutions.[1–4] More recently studies have begun along the same lines on crystallizing polymers with the aim of assessing the conformation and structure of a given molecule within its own crystalline environment.

There are a number of questions concerning crystalline polymers to which there have not hitherto been conclusive answers, and it is to these that the neutron-scattering technique promises to make substantial contributions. It should, however, be stressed that the technique has some inherent limitations which it shares with scattering techniques in general and low-angle scattering in particular. It may not be superfluous to reiterate that no scattering analysis can be entirely self-contained. Thus the scattering pattern per se cannot tell us what the scattering elements are and therefore other available knowledge on the scattering entities needs to be utilized. This is necessary in order to obtain a meaningful answer to the more specific questions being asked about the entities of interest, and also in order to discriminate between signals which are due to the entities of interest and those which may not form the subject of the particular enquiry but may nevertheless contribute to the scattering. For this reason, the existing knowledge relating to our systems will be briefly summarized; this is folllowed by the listing of the type of signals which might be expected as a result.

Linear polyethylene is known to be substantially crystalline.[5,6] The width of the wide-angle x-ray reflections indicates sizes of coherently diffracting crystals in the range of hundreds of ångströms in the three crystal directions. This implies the presence of straight-chain segments ("stems") of this magnitude within the crystallites, which, accordingly, will have to be the basic chain constituents of the systems to be studied here.

When formed in solutions the basic morphological crystal entities are readily accessible, and, as is well known, are the familiar "single-crystal" lamellae. Even if the corresponding identification in the more compact melt-crystallized systems is not as readily achieved, analogous lamellar entities are recognizable even in this case. It may not be extraneous to the present paper to provide two recent illustrations of such lamellar organizations in melt-crystallized material under two different conditions of crystallization (Figure 1 kindly provided by Dr. D. T. Grubb of this laboratory) as these display structures such as the samples of the present investigation are likely to contain on the level of the electron microscope. Thus, except perhaps for specially effective quenching procedures[9] for which not surprisingly all types of electronmicroscopic morphology may become indistinct,[10] we can add the lamellae to the known basic constituents of the samples under consideration. Low-angle x-ray scattering, wide-angle x-ray line-width analysis,[11] and low-frequency Raman spectroscopy (e.g., 8) provide additional evidence on this lamellar structure. The basic lamellae are the building stones for larger scale structures. For crystallization from solution these are the various multilayer aggregates and for melt crystallization they are the spherulites, both readily observable under the optical microscope. These form a hierarchy of entities which are all contained in samples used for the present type of neutron scattering experiments and therefore need taking note of in the evaluation of the signals.

On the molecular level it is the path of a given chain through the lamellar units which is both a matter of considerable interest and one to which the new technique should provide uniquely new information. This of course comprises the issue of chain folding. In this connection it needs remembering that the existence of lamellae with the straight-chain segments perpendicular (or nearly so) to the lamellar surface implies folding by necessity. If the lamellae are entirely separate entities the full chain must keep refolding within the same layer. But even if lamellae are contiguous (as, e.g., in Figure 1a), a certain amount of folding back must still exist owing to space-filling considerations at the crystal interfaces. In addition, solution-grown crystals, which are more amenable to individual examination, provide a variety of indications for varying degrees of coordination in the mutual arrangement of the fold segments (e.g., sectorization[5,6]) which, among other indications, raise the issue of the adjacency of the fold reentry, one of the principal enquiries of the present work.

As concerns the signals to be expected we may for convenience list the following three sources of contrast, which may contribute to the scattering at the various ranges of angle as discussed below.

Individual Molecules of Contrasting Isotope. The recording of the corresponding scattering function has of course been the initial objective of this kind of neutron-scattering work. This may be modified by lack of randomness of the arrangement of centers of gravity of labeled molecules. However, such modifications may become negligible at sufficiently large angles.

Crystal Lamellae. On these neutron scattering provides no new information; by choosing a matrix of hydrogenous polyethylene (HPE) this may be avoided almost entirely, and for a matrix of deuteriopolyethylene (DPE) it may be avoided by measuring at sufficiently large angles.

Structures on the Scale of Microns. These may cause scattering; as examples we may cite crystal aggregates and cracks between them. The scattering length density may well vary across the aggregates; this may be considered as a particular case of lack of complete dispersion of one isotope species in the other (see later).

These three sources of scattering should be related to corresponding distances s from the origin in reciprocal space ($s = 2 \sin \theta/\lambda$ where 2θ is the scattering angle and λ is the wavelength). It is useful to define two regions of s:

(a) $s < 10^{-2}$ Å^{-1}. If the only source of scattering is randomly dispersed labeled molecules, a radius of gyration should be obtainable. However, there may well be a contribution from lack of randomness which may be related to crystal aggregates (see below). Contributions from aggregates should be most important for s about 10^{-5} Å^{-1}, but a significant degree of scattering is likely to extend to larger s.

(b) $10^{-1} > s > 10^{-2}$ Å^{-1}. Molecular detail, in particular the mode of folding, should affect the scatter in this angular range directly. In the case of liquid solutions and amorphous polymers such effects have already been tested by measurements in this range[3,4] (sometimes referred to as the "intermediate range").

Past work on melt crystallization comprised both ranges (a) and (b)[12-14] while the only work on solution-grown crystals by ourselves has been confined to range (b).[15] Not only are the conclusions of ref 15 distinctly different from those in 14 by the analysis in ref 16, but even the validity of these conclusions is being doubted.[14] In the light of these differences (to be referred to again more specifically in the Discussion) the present paper addresses itself to the task of combining work on melt and solution crystallized material comprising all relevant angular ranges, in a comparative manner.

Out of the full angular range (b) (molecular detail) will be our main concern. Nevertheless, cognisance will be taken of scattering also at smaller angles, partly because this is relevant to information about large-scale structures ("aggregates") and partly because they have some new information to convey on the potential limitations of this type of neutron-scattering method in general. It is to be stated that the present work does not purport to be a systematic study on the relation between radius of gyration and molecular weight obtainable from range (a); data relating to this range serve primarily to safeguard the conclusions in the rest of the paper.

Crystalline polymers are not in equilibrium, and there are a large number of variables depending on, e.g., thermal history. This complexity makes difficult a complete and systematic investigation with respect to all variables. Hence this report constitutes a series of measurements, the choice of which depended on the development of the study at any particular time, and also on external constraints such as availability of facilities. Nevertheless we consider that the sum total of the information announced here should be amply sufficient to justify the conclusions drawn.

Methods

Specimen Preparation. Deuteriopolyethylene (DPE) and the hydrogenous polymer (HPE) of specified molecular weights (determined by gel permeation chromatography, GPC) were blended by stirring in simmering xylene for at least 2 h. The solutions were then poured into thin-walled glass tubes held variously at 85 °C, 78° C, 70 °C, and room temperature. The crystals were filtered and dried to form mats, the last part of the drying being carried out under vacuum. The crystal mats were either pressed (in order to remove voids)[15] or melted at about 150 °C and recrystallized. The crystallization from the melt was in the form of thin films, which were either quenched into water or cooled at about 1 or 10 °C/min. For reasons to become apparent later, some samples were irradiated by γ rays to a dose of 50 Mrad (by Dr. P. Fydelor of the Royal Military College, Shrivenham). These samples were then recrystallized by melting to the rubbery state and by subsequent cooling at a rate of about 1 °C/min. Isotope concentrations were monitored by infrared (IR), and, in some cases of DPE matrix, by measurements of the (angularly independent) incoherent neutron scattering. No evidence for loss of deuterium during sample preparations was detected (cf. ref 12). Crystal orientation textures in the case of single crystals was defined by x-ray diffraction.

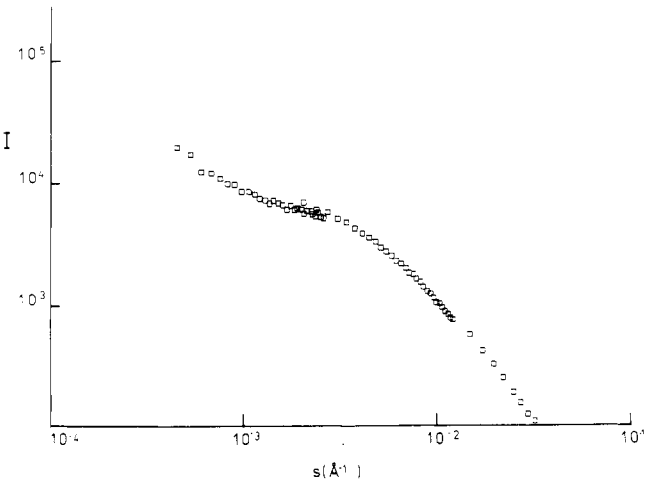

Figure 2. An example of a scattering signal after corrections for backgrounds as explained in the text. The sample (solution crystallized) is described in Table I (No. 12). The data are derived from three different camera settings (distances 0.6, 2.5, and 10 m).

Neutron-Scattering Methods. The low-angle facility[17] at the Institute Laue Langevin (Grenoble) was used with several camera distances from 0.6 to 20 m. The samples, which were in the form of sheets of thickness about 0.1 to 0.5 mm and area 100 mm^2, were stacked in sample holders of either aluminum or quartz so as to achieve a total thickness in general between 0.5 and 1 mm. The background corrections were made on the basis of measurements on the sample blend, on the empty cell, on the cell containing a cadmium mask, and on a series of specimens of pure HPE and DPE of differing thickness, together with measurements of the attenuation of the incident beam by the specimens. Measurements were carried out in range (a) ("small angles"), using HPE matrix, and in range (b) ("large angles"), using HPE and DPE matrix. The subtraction of the incoherent signals from HPE was made on the basis of incoherent scattering from pure HPE of the same weight as the HPE component of the blend. In the case of HPE matrix the coherent background was also assumed to be that of a pure HPE sample of the same weight; this was identified as a small contribution at s about 10^{-3} Å^{-1}. In the case of the DPE matrix the coherent background was assumed to be the same as that from the same weight of pure DPE as in the blend; this contribution was also small compared with the difference signal in the relevant range of s (0.02 to 0.06 Å^{-1}). A small but significant diffuse signal associated with DPE was also identified. The background levels were checked further by measurements in the angular range intermediate between range (b) and the position of the 110 wide-angle maximum, using the diffractometer at Harwell.[18] The DPE matrix samples have low enough background signals to enable a difference signal to be obtained for a label concentration as low as 1% to an equivalent Bragg spacing of 16 Å. Corrections were made for variations in counter response.

Intensities were calibrated with reference to the scattering from vanadium. The incoherent scattering from HPE was used as a secondary standard. A corrected scattering curve is shown in Figure 2.

Methods of Analysis. A number of well-established analyses have been employed in order to understand the basic nature of the scattering. Radii of gyration could, in certain circumstances, be derived from either of eq 1 or 2

$$I = I_0 \exp(-4\pi^2 R_g{}^2 s^2/3) \quad (1)$$

$$I_0/I = 1 + 4\pi^2 s^2 R_g{}^2/3 \quad (2)$$

where R_g is the radius of gyration, and where I the normalized

intensity is related to the usual differential cross sections $d\Sigma/d\Omega$ by

$$I = \frac{d\Sigma}{d\Omega} V/\{4\pi n(b_D - b_H)^2\}$$

Here n is the number of "label" nuclei in the sample, V is the sample volume, and b_D and b_H are the scattering lengths of deuterium and hydrogen. In these units $I_0 = M/8$, where M is the effective molecular weight of DPE in an HPE matrix.

For either of eq 1 or 2 to give an R_g value relevant to a single molecule the centers of gravity of the molecules must be randomly arranged. A test for this condition is whether the measured I_0 correlates well with the known value of M_w from GPC and whether plots of log I against s^2 (eq 1) or $1/I$ against s^2 (eq 2) give linear plots. Equation 2 was derived specifically for polymer coils in solution, whereas the value of s at which eq 1 fails to be a good approximation will be largest for compact globular structures.[19] While the structure within the crystals cannot possibly be a coil, another structure which is far from being compact may also yield scattering which is approximated to larger s by eq 2 than by eq 1.

Equations for range (b) at sufficiently large s, i.e. s large compared with $1/l$ where l is the stem length, are related to the scatter of what is the basic "subunit" of the molecule. By subunit is meant either straight rows of stems (chain traverses through lamellae) or individual stems. These correspond to predominantly adjacent and random fold re-entry, respectively. Rows of stems constitute sheets for which the scattering is given by[15,19]

$$I = (n_A/2\pi s^2 \cos\theta) \exp(-4\pi^2 D^2 s^2) \quad (3)$$

where n_A is the number of deuterium nuclei per unit area of lamellae, and $D^2 \equiv \overline{Z^2}$ where Z is the perpendicular distance of nuclei from the center plane of the lamellae.

Individual stems constitute rods for which the scatter is

$$I = (n_L/2s \cos\theta) \exp(-2\pi^2 R^2 s^2) \quad (4)$$

where n_L is the number of nuclei per unit length of rod and $R^2 \equiv \overline{r^2}$ where r is the distance of each nucleus from the center line of the rod.

Both eq 3 and 4 differ from their equivalents in ref 19 (eq 41 and 40) since the intensity in our case is normalized with respect to the number of scattering nuclei (e.g., D in HPE). In ref 19 the normalization is with respect to the number of lamellae or rods; it is for this reason (and no other) that in the limit of large s the equations in ref 19 contain a dependence on the rod length and the lateral lamellar width. The factors of $\cos\theta$ are included for completeness; in the low-angle limit they can be omitted and the form found in ref 19 results. In practice $\cos\theta$ can be taken as unity for all the results here.

Experimental data can be tested against eq 3 and 4 by plotting either Is^2 or Is on a log scale against s^2. We found that expressing the scattering in range (b) in this way was helpful in interpretation; in particular the primary dependence of this intensity on the subunit structure rather than on the long-range chain conformation emerges clearly from this procedure.

If structures are present whose size is large compared with the equivalent Bragg spacing ($1/s$), an s^{-4} dependence of scatter can be expected

$$I(n/V) = (\Delta\rho)^2 A/(8\pi^3 s^4) \quad (5)$$

where, in the units given above, $\Delta\rho$ is the deuterium density difference between the interior and exterior of the structures, A is the surface area per volume of sample, and n/V is the overall density of deuterium in the sample. For completely random mixing of isotope (as is usual for liquid solutions) $\Delta\rho = 0$. Since aggregates on the scale of microns are known to exist in crystalline polymers, and if $\Delta\rho$ is not zero for any reason, a contribution to the intensity will be made. Equation 5 will be a good approximation to this contribution if the deuterium density distribution is represented by two density levels, whose difference is $\Delta\rho$.

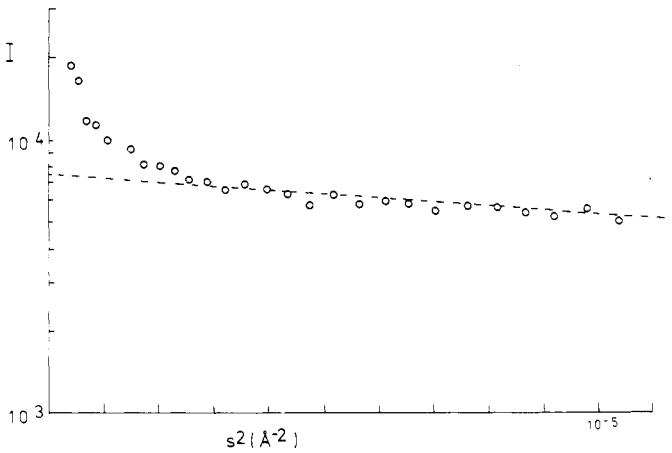

Figure 3. Part of the data which are shown in Figure 2 (solution crystallized, sample 12 of Table I) plotted according to eq 1.

Equations 1–4 all refer to the coherent scatter from dispersed labeled molecules (the first source of intensity listed in the first section); any contribution from eq 5 will be additional to this in the same way that low-angle scattering is additional to the wide-angle scatter in more conventional scattering experiments (e.g., by x rays).

The finite degree of monochromatization will produce a readily predictable modification to the intensities, as long as an analytic variation of I (e.g., eq 1–5) is obeyed over an extended region of s. In particular, a Gaussian variation of true intensity with s will give an observed Gaussian dependence of I but with an "effective wavelength" which differs from the wavelength at the peak in the wavelength distribution.[3] Similarly a variation of true intensity of the type Ks^{-n} will give a variation of observed I as $K's^{-n}$, but with a modified constant K'. These effects are small as long as the wavelength selector on the low-angle spectrometer gives a wavelength distribution of 8% fwhm (full width of half maximum), i.e., using the monochromator known as "Brunhilde" (B).[17] Some measurements in range (a) were carried out using a wavelength distribution of 40% fwhm (monochromator "Adele" (A)). This gives rise to some uncertainties in some of the measured parameters calculated from the scattering curves, since, in particular, the type of scattering at s values less than that corresponding to the lowest measured angles is not known.

Results

The general approach of this work is to systematize a large number of measurements in as coherent a way as possible in the light of existing knowledge of the systems. In line with this initially rather descriptive method of reporting the results, data have been plotted according to eq 1–5. Certain generalizations will be made as to whether straight-line plots were obtained and, further, whether the resulting slopes and intercepts are reasonable on the basis of these methods of analysis. The following section will give a more detailed interpretation.

When measurements were made at sufficiently small angles, plots according to eq 5 usually yielded fairly straight lines; the slopes of these lines differed widely, however, the intensities being very much higher for samples crystallized at low supercoolings. Meaningful plots according to eq 1 and 2 could only be obtained for samples crystallized at high supercoolings. Plots according to eq 3 and 4 showed consistent varia-

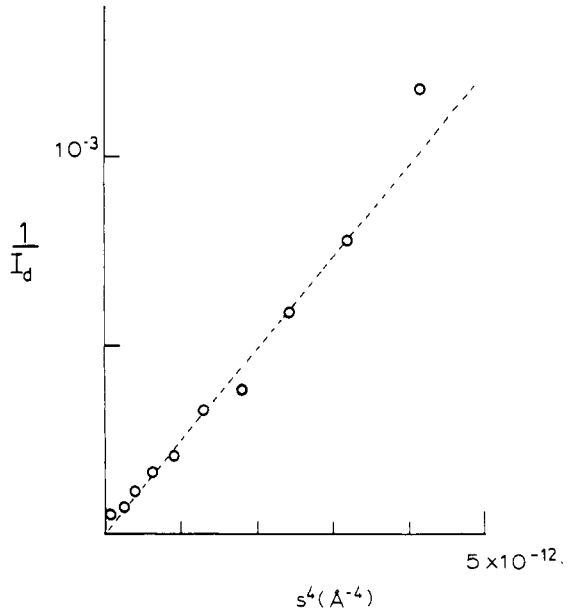

Figure 4. Difference intensity I_d which is taken from data such as shown in Figure 3 as explained in the text, corresponding to sample 5 of Table I. It is plotted according to eq 5.

tions according to whether the growth was from solution or from the melt and also according to molecular weight.

Angular Range (a) ($s < 0.01$ Å^{-1}). Solution-Grown Crystals. It was found that in most of the cases where data were available down to $s = 7 \times 10^{-4}$ Å^{-1} (equivalent Bragg spacing 1400 Å), straight-line plots could be obtained by using

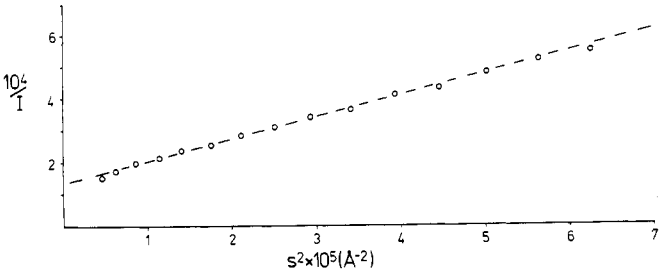

Figure 5. Part of the data which are shown in Figure 2 (sample 12, solution crystallized, of Table I) plotted according to eq 2.

eq 1, 2, or 5 or by a combination of these. Figure 3 shows a representative Guinier plot with a well-defined linear region. There is however an upswing in intensity above this line for $s^2 < 5 \times 10^{-6}$ Å^{-2}. The intensity in this region was plotted according to (5). Figure 4 shows a typical result; in this case the intensity I_d used for Figure 4 is derived from a signal of the type shown in Figure 3 by taking the difference between the observed intensity and the line extrapolated from larger s. In many cases of large I_d subtraction represents only a small correction.

Table I is a summary of a number of measurements; here columns 1–5 refer to sample types, 6 and 7 refer to the conditions of the scattering experiments, and 8–14 contain the results. Seven samples gave linear Guinier plots over a range of s similar to that shown in Figure 3. In those cases, where the plots were verified as linear, not only the intercept intensity I_0 is quoted (which should then give a measure of the number of deuterium nuclei in each scattering entity) but also an "effective molecular weight" (M_{eff}) is calculated. It will be seen

Table I
Summary of Results on Solution-Grown Crystals in Range (a) ($s < 0.01$ Å^{-1})[a]

Sample No.	Mol wt DPE × 10⁻³	Wt fract of DPE × 10²	Mol wt HPE × 10⁻³	Temp of cryst, °C	Min value of s, Å^{-1}	Monochromatization	Eq 1 I_0 × 10⁻³	Eq 1 M_{eff} × 10⁻³	Eq 1 R_g, Å	$(\Delta\rho)^2A$ × 10¹⁰, Å^{-4}	Eq 2 I_0 × 10⁻³	Eq 2 M_{eff} × 10⁻³	Eq 2 R_g, Å
1	11.4	1	7	70	7 × 10⁻⁴	A	23						
2	22	1	7	70	7 × 10⁻⁴	A	3.6			10			
3	47	1	7	70	7 × 10⁻⁴	A	5.4	43		14			
4	59	0.22	7	70	7 × 10⁻⁴	A	5.8	46					
5	59	0.6	7	70	1.2 × 10⁻³	B	4	32	51				
5	59	0.6	7	70	7 × 10⁻⁴	A	4.6	37		4			
6	59	1	7	70	7 × 10⁻⁴	B	5.3	42	65	56			
7	59	10	7	70	7 × 10⁻⁴	A	111			762			
8	11[b]	0.45	109	70	3 × 10⁻³	B	3.9				4.5		
9	11[b]	0.45	109	85	3 × 10⁻³	B	12						
10	29[b]	5	109	70	3 × 10⁻³	B	15.5						
11	29[b]	5	109	85	3 × 10⁻³	B	41						
12	39[b]	1.4	109	70	7 × 10⁻⁴	B	7.5	60	53	1.4	7.6	61	62
13	39[b]	7	109	70	7 × 10⁻⁴	B	7.8	62			9.3	74	60
14	39[b]	1.4	109	85	7 × 10⁻⁴	B	9.5			220			
15	63[b]	4	109	70	7 × 10⁻⁴	B	9	72	50	30	7.6	61	58
16	63[b]	4	109	85	3 × 10⁻³	B	34						
17	260[b]	4	109	70	3 × 10⁻³	B	22				20		
18	207[c]	13	109	70	3 × 10⁻³	B					13	106	
19[d]	207	10	109	70	7 × 10⁻⁴	B				1900			

[a] The first five columns define the sample conditions, the next two the camera setting, and the last seven the results. A and B refer to wavelength selectors (see text) of 40% and 8% fwhm wavelength distribution. The results were obtained from the data by the use of eq 1, 2, and 5 as explained in the text. Sample 12 refers to the data shown in Figures 2, 3, and 5 (corresponding measurements are also shown in Figure 7). DPE was provided by Merck Sharp and Dohme. The DPE fractions were made in two ways. [b] Obtained in small quantities using an analytical GPC. These molecular weight values are estimated *peak* molecular weights by GPC. GPC analysis of such samples indicates a ratio M_w/M_n of about 1.5, the M_w value being slightly higher than the molecular weight at the peak of the chromatogram. Other fractions were obtained by fractional crystallization, and the molecular weight values refer to M_w (by GPC). M_n values are as follows: sample 1, 7700; 2, 14 000; 3, 31 000; 4–7, 31 000; 4–7, 31 000. [c] Sample 18 refers to unfractionated DPE (M_w = 207 000, M_n = 75 000). The matrix (HPE) was either "Rigidex 2" (M_w = 109 000, M_n = 18 000) or a low molecular weight fraction which had a similar dissolution temperature in xylene to that of the DPE fractions (M_w = 6800, M_n = 5200). [d] For this sample the HPE was crystallized first, and a solution of DPE was added to the crystal suspension and allowed to crystallize. Subsequently the sample preparation was similar as for the other samples.

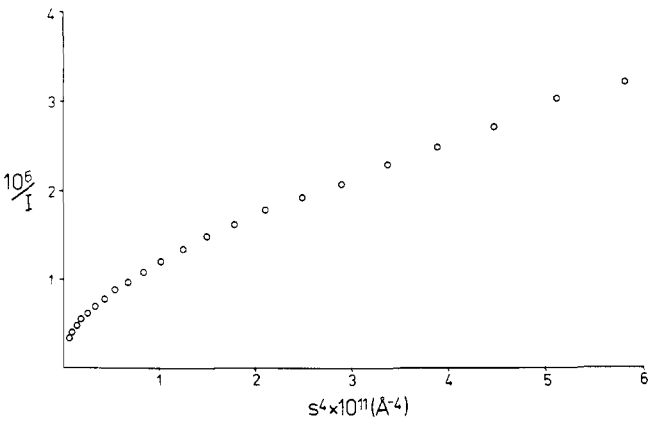

Figure 6. Data corresponding to sample 1 of Table II (crystallized by cooling from the melt at 1 °C/min). I in this case is the total scattering associated with the DPE (cf. Figure 4). The plot is in accordance with eq 5.

that for these seven examples the agreement between M_w by GPC and neutron scattering was well within a factor of 2 (sample numbers 3, 4, 5, 6, 12, 13, and 15).

A number of other data are available where either the measurements did not include low enough angles to construct a complete plot according to (1) (these data were however sufficient to estimate I_0) or the plots were far from linear. Table I therefore includes the corresponding I_0 values, for which however an effective molecular weight is not calculated. In several cases I_0 is unrealistically large, notably when crystallization is at 85 °C (samples 9, 11, 14, and 16). Several such cases were however observed also for crystallization at 70 °C (samples 1, 2, and 7) where the plots were far from linear. In these cases a rough estimate of I_0 is made by constructing a tangent to the data curves at s^2 about 8–10 × 10^{-6} Å^{-2}.

As stated earlier determination of R_g was not our primary object, nevertheless where these could be derived with confidence such as in Figure 3 the data are placed on record. This is confined to cases where the monochromatization was sufficiently good (8% fwhm) and in addition where a linear slope was clearly definable.

Data of the type shown in Figure 3 gave straight lines (for corresponding values of s^2) when plotted as $1/I$ (eq 2), as they should since eq 1 and 2 are equivalent at small enough values of s. However, in addition, it was found that straight lines according to (2) were obtainable to quite high values of s^2 (Figure 5), even for crystallization at 85 °C, and even when the parameters I_0 and R_g were not physically reasonable when compared with the range of equivalent Bragg spacings. Hence we have used data such as in Figure 5, but with some discretion; as shown in Table I this enables several additional R_g values to be obtained from the parts of the scattering curves where eq 1 is no longer obeyed.

Sample 18 was the *same* sample as used previously;[15] although the DPE was not fractionated, the I_0 value corresponds approximately to the M_w by GPC.

Values of $(\Delta\rho)^2A$ which are derived from plots according to eq 5 are also included in Table I. These values are highly variable and are particularly large for crystallization at 85 °C. A very large value of $(\Delta\rho)^2A$ was obtained for crystals which were grown by adding 10% by weight of DPE in the form of solution *after* the HPE had fully crystallized (sample 19). This sample consists therefore of intimately mixed crystal regions of pure HPE and DPE.

Melt-Crystallized Samples. The same general results were obtained as for single crystals, in particular with regard to the effect of supercooling, though the data are less extensive. In addition the plots according to (5) are not as linear as for solution growth (Figure 6). Only two results were obtained which gave linear plots according to (1); the corresponding extrapolated intensities of these samples are quoted in terms of effective molecular weights in Table II (samples 2 and 3). They are comparable with the estimated molecular weights within at least a factor of 2. The other values for zero angle intensities are evaluated from tangents drawn to concave plots; they can have therefore little direct physical significance. The values for $(\Delta\rho)^2A$ are variable and rise to a very high value in the case of slow cooling. An irradiation treatment after quenching but prior to remelting and recrystallizing by slow cooling gives however a considerably reduced value of $(\Delta\rho)^2A$ (compare samples 9 and 1).

Angular Range (b) ($s > 0.01$ Å^{-1}). The aim of these experiments was to test eq 3 and 4, i.e., whether the basic unit of folding is a sheet (i.e., rows of stems) or a rod (i.e., isolated stems). For this reason the data are displayed as Is (for rods) or Is^2 (for sheets) on a log scale vs. s^2. Much of the data refer to results with a DPE matrix (this reduces background as discussed above). Results were also obtained with HPE ma-

Table II
Summary of Results on Melt-Grown Crystals in Range (a) ($s < 0.01$ Å^{-1})[a]

Sample	DPE mol wt × 10^{-3}	HPE mol wt × 10^{-3}	Wt fract of DPE × 10^2	Cryst conditions	Min value of s, Å^{-1}	Monochromator	I_0 × 10^{-3}	M_{eff} × 10^{-3}	R_g, Å	$(\Delta\rho)^2A$ × 10^{10}, Å^{-4}
1	59	109	1	Cooling at 1°/min	7 × 10^{-4}	A				36 × 10^3
2	39[b]	109	1.4	Quench	7 × 10^{-4}	B	5.5	44	100	11
3	107[b]	109	1	Quench	7 × 10^{-4}	B	8.3	66	160	20
4	59	109	1	Quench	1.2 × 10^{-3}	B	19			
5	59	3.5	1	Quench	7 × 10^{-4}	A	13			10
6	59	109	5	Quench	7 × 10^{-4}	A	10			
7	59	3.5	1	Quench	1.2 × 10^{-3}	B	12.5			60
8	59	3.5	1	Isothermal crystalization at 114 °C	7 × 10^{-4}	A	22			
9	59	109	1	Quenched, irradiated, recrystallized by cooling at 1°/min	7 × 10^{-4}	A	40			80

[a] Molecular weight fractions and other experimental details are explained in the footnotes to Table I; in addition the matrix material for samples 5, 7, and 8 gave M_w = 3500, M_w = 2600 (this fraction had a similar melting point to the DPE fractions). The results were obtained from the data by use of eq 1, 2, and 5 as explained in the text. Sample 1 refers to data in Figure 6. [b] See Table I.

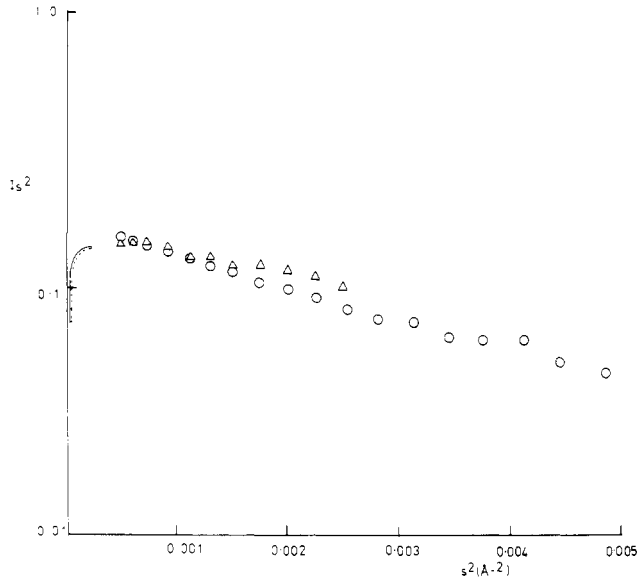

Figure 7. Data from range (b) ($s > 0.01$ Å^{-1}) for HPE matrix, corresponding to samples 12 (Δ) and 13 (○) of Table I. The intensities (which are normalized) agree for the two DPE concentrations of 1.4 and 7% which are shown. The plot corresponds to eq 3. The systematic errors are probably large compared with the statistical errors. Two camera settings were used; those measurements made at smaller s (longer camera distance of 2.5 m) are shown by continuous curves, the results for DPE concentration of 7% being shown by a broken curve.

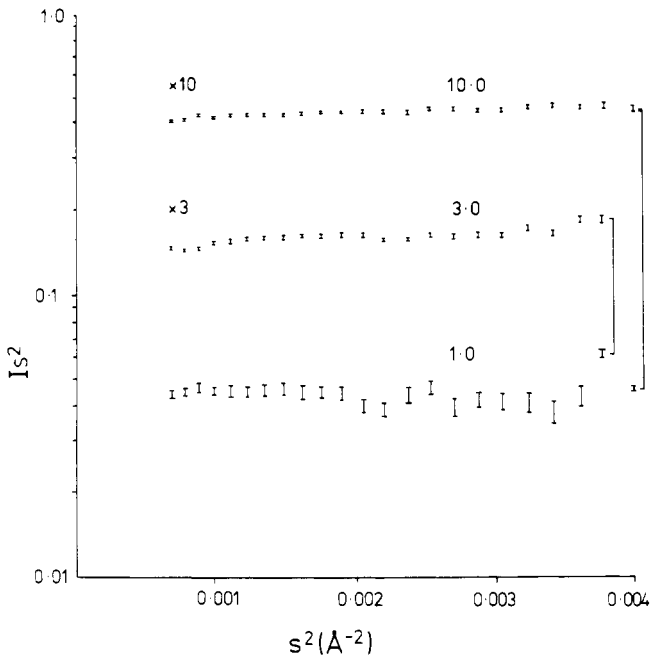

Figure 8. Data from range (b) ($s > 0.01$ Å^{-1}) for DPE matrix corresponding to samples referenced as No. 1 in Table IV (solution crystallized at 70 °C, M_w of HPE = 5200) plotted according to eq 3. The figure shows several concentrations of HPE: the concentrations in percentages are 1.0, 3.0, and 10.0 (as marked). These intensities are displaced for clarity as shown by the vertical lines and by the factors ×3 and ×10. Statistical errors are shown by the bars.

trix, mainly on solution-grown crystals. An advantage of using the HPE matrix is that measurements in range (a) can also be made. This serves an important purpose, namely to assess whether there is any departure from complete dispersion of the isotopic species, and, if yes, whether this has any influence on the measurements in range (b). We would stress that there is a second test of the validity of using eq 3 and 4, namely the comparison of normalized intensities from samples with different label concentrations.

Figure 7 shows two examples of data with HPE matrix, corresponding to samples 12 and 13 in Table I. One of these also features in Figures 2 and 3. This agrees well with the previously published results[15] using unfractionated DPE (sample 18, Table I). Is^2 decreases with s^2.

The above results are corroborated by a number of samples of single crystals (Table III). The results listed in this table are described by values of n_A and D, which, according to eq 3, are defined by intercept and slope, respectively. The data in Figure 7 refer to sample 1 of Table III. For other samples which are listed in the table, a similar decrease of Is^2 toward small s^2 for $s^2 < 0.0002$ Å^{-2} is observed as in Figure 7. There would seem to be much less variability in this range of s than in range (a), and in particular the differences according to supercooling are smaller. Crystallization at 85 °C gives smaller values of n_A compared with crystallization at 70 °C.

Results using DPE matrix are described in Figures 8–10 (solution growth) and Figures 11–14 (melt growth). Because of small background signals, results were obtainable down to small HPE concentrations (0.3% in one case). In normalized units of intensity there is very little concentration effect (intensity values are deliberately displaced in the figures for clarity) in the ranges observed (10 to 0.3% for solution growth, 10 to 1% for melt growth) (Figures 8, 9, 11, and 12).

There is a marked difference in the results for solution-grown and melt-grown crystals, in so far as both the absolute value of Is^2 and the dependence of Is^2 on s^2 is quite different for a given molecular weight (compare, e.g., Figures 10 and 13).

Table III
Summary of Results on Solution-Grown Crystals in Range (b) ($s > 0.01$ Å^{-1}) Using a Matrix of HPE[a]

Sample No.	Mol wt of DPE × 10^{-3}	Wt fraction of DPE × 10^2	T_x, °C	n_A	D, Å
1	39	1.36	70	1.2	2.4
2	39	7	70	1.1	2.7
3	39	1.36	85	0.7	4.8
4	63	5	70	1.6	3.1
5	63	5	85	0.84	3
6	107	9	85	0.6	2.5
7	260	4.5	70	2	2.1
8	260	4.5	85	1.3	3.4
9	316	4	70	1.5	3.2
10	549	3	85	1.8	2.7
11	1000	2	85	1.8	2.7

[a] The matrix of HPE has M_w = 10 900, M_n = 10 000. Labels were DPE (GPC fractions, see Table I). The results were obtained from eq 3 as explained in the text. Sample 1 refers to data in Figure 7 (also sample 12 of Table I).

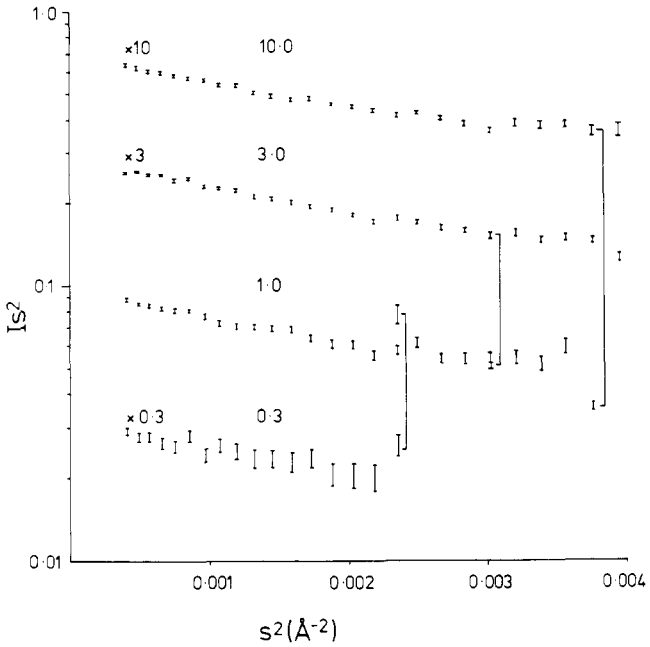

Figure 9. Plots similar to Figure 8, for the samples referenced as No. 4 in Table IV (M_w of HPE is 31 000).

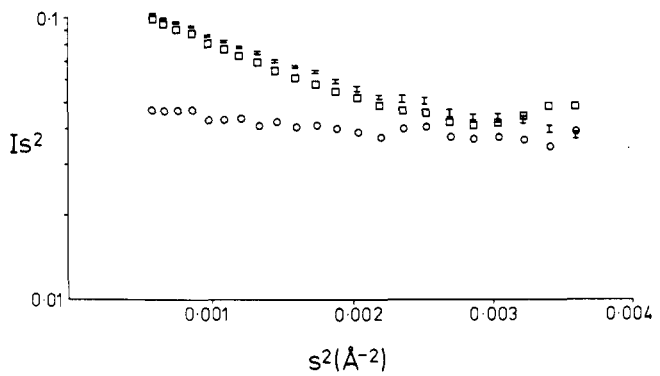

Figure 10. Data from range (b) for DPE matrix, crystals grown at 70 °C from solution: (○) ref 2 (Table IV, M_w = 10 200); (I) ref 5 (Table IV, M_w = 97 000); (□) ref 7 (Table IV, M_w = 271 000). The plot is according to eq 3; statistical errors are all similar, for a given s, to those shown by the one set of data using bars (M_w = 97 000).

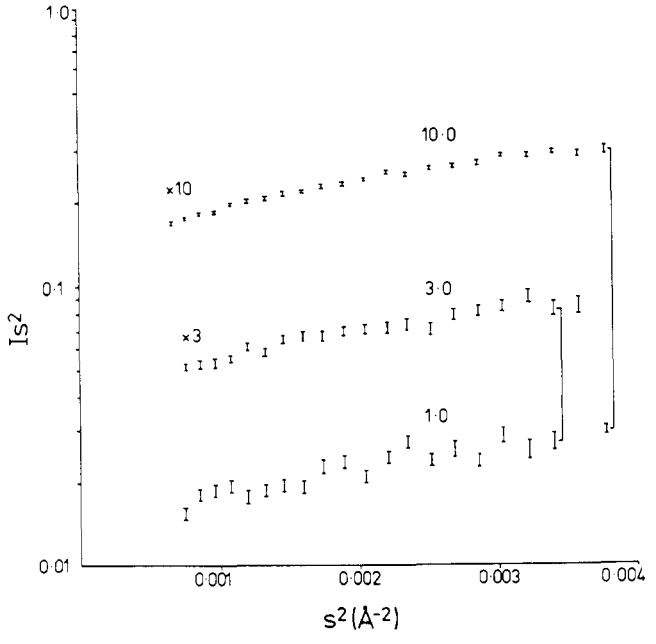

Figure 11. Data from range (b) for DPE matrix, melt-crystallized samples, M_w of HPE being 5200 (ref 9 of Table IV). The method of plotting is explained for Figure 8.

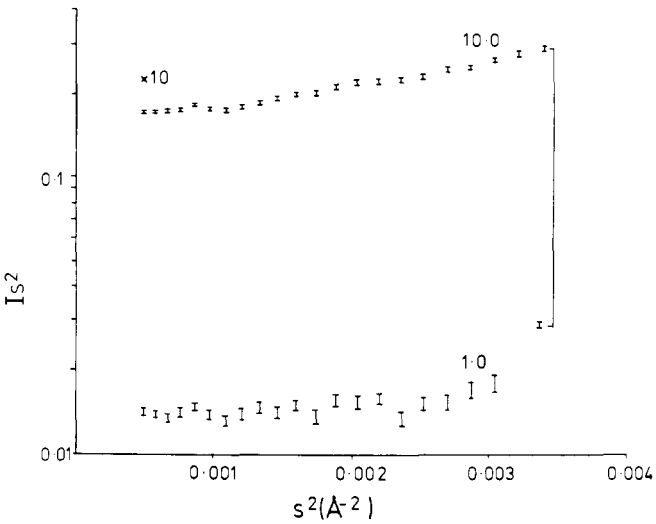

Figure 12. Data from range (b) for DPE matrix, melt-crystallized samples, M_w of HPE being 31 000 (ref 11 of Table IV). The method of plotting is explained for Figure 8.

For solution-grown crystals the plots are linear, the slopes of the lines increasing with molecular weight. For melt-grown crystals the plots are distinctly nonlinear for small molecular weight, and for high molecular weights Is^2 tends to be constant.

Results for melt-grown crystals were also plotted as Is vs. s^2 (Figure 14) where the data points could be described, at $s^2 > 0.0015$ Å^{-2}, by lines with negative slopes. The data in the figures are summarized in Table IV, since in the cases where straight lines are observed n_A, D, n_L, and R values can be calculated. Data are also included for crystals grown from solution at 78 °C (these data are not shown in the figures). For solution-grown crystals, analagous results for HPE and DPE matrix samples can be compared (Tables III and IV). The two sets of data are comparable (results in Table IV being much more precise). Samples 1–3 (approximate molecular weight 39 000, Table III) would seem to show similar behavior to samples with higher labeled molecular weights, as compared with a label molecular weight of 31 000 (Table IV).

Interpretation and Discussion

The value of this technique depends on a clear identification of a signal with its physical origin. In general this has posed few problems in the case of blends of hydrogenous and deuterated polymers in the liquid or solution form, where radii of gyration have been unambiguously derived. Equally, data in the "intermediate" region, i.e., $s > 0.01$ Å^{-1}, have also been obtainable.

Considerable difficulty has, however, been encountered in the case of polyethylene blends in the crystalline state, the symptoms being scattering toward low angles (i.e., range (a)) which is in excess of that expected from homogeneous blending. This excess intensity which has been attributed to "clustering" [13] has seriously interfered with attempts to assess the radius of gyration. From the onset this "clustering" was attributed to the known melting point differences between the isotopic species. Methods used to eliminate it included melting point matching by the use of branched species of one of the components and fast cooling from the melt.[14]

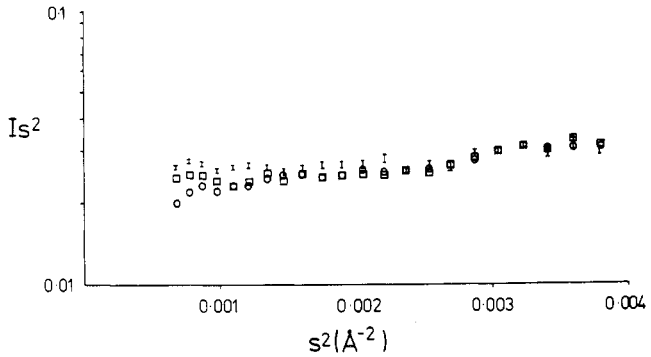

Figure 13. Data from range (b) for DPE matrix, melt-crystallized samples: (○) ref 10 (Table IV, M_w = 10 200); (I) ref 12 (Table IV, M_w = 9 700); (□) ref 13 (Table IV, M_w = 271 000). The plot is according to eq 3; statistical errors are all similar, for a given s, to those shown by the one set of data using bars (M_w = 97 000).

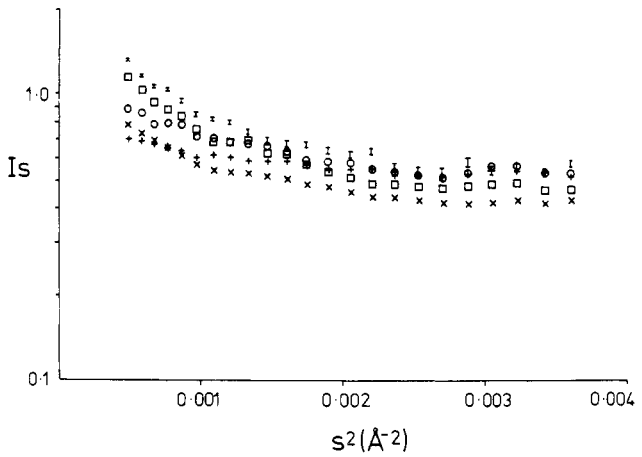

Figure 14. Data from range (b) for DPE matrix, melt-crystallized samples, plotted according to eq 4: (+) ref 9 (Table IV, M_w = 5 200); (○) ref 10 (Table IV, M_w = 10 200); (×) ref 11 (Table IV, M_w = 31 000); (I) ref 12 (Table IV, M_w = 97 000); (□) ref 13 (Table IV, M_w = 271 000). Statistical errors are all similar, for a given s, to those shown by the bars.

In the angular range (b), i.e., $s > 0.01$ Å^{-1}, the identification of the signals appeared to be more straightforward, the scattering unit considered being no longer a whole molecule but constituent elements of the molecule itself. By use of eq 4 past work on single crystals[15] identified these elements as sheets which are one molecule thick ($D \sim 1.6$ Å) with a deuterium density per unit area corresponding to the fully deuterated molecule. This leads to the picture where the scattering unit is a chain-folded ribbon with the adjacent stems belonging to the same molecule, hence where folding is adjacently re-entrant. At the time of this work on single crystals the issue of excess intensity in range (a) had not yet arisen. Subsequently, doubt was cast on it[14] as on all potential neutron-scattering work of its kind, where the absence of this excess intensity has not been explicitly ensured. This doubt has been implicitly reinforced by concurrent works on melt-crystallized samples in this angular range (b) where the analysis of the results indicated that the scattering unit is closer to isolated fold stems than to sheets,[14,16] an effect also being indicated by our own preliminary results at the time.[20] Hence the objectives of the present investigations are as follows: (1) are the results on the sheet nature of the scattering entities upheld in the case of solution-grown single crystals, even when the absence of excess

Table IV
Summary of Results in Range (b) ($s > 0.01$ Å^{-1}) Using a Matrix of DPE[a]

Ref	HPE $M_w \times 10^{-3}$	HPE $M_n \times 10^{-3}$	Wt fraction of HPE × 10²	Temp of crystallization, °C	n_A, Å^{-2}	D, Å
			Solution-Grown Crystals			
1	5.2	4.5	1, 3, 10	70	1.8, 3, 1.6	0, 0, 0
2	10.2	8.5	3	70	0.28	1.4
3	10.2	8.5	3	78	0.21	1.7
4	31	28	0.3, 1, 3, 10	70	0.58, 0.61, 0.60, 0.53	2.1, 2.4, 2.4, 2.6
5	97	86	3	70	0.81	3.2
6	97	86	3	78	0.39	1.9
7	271	200	3	70	0.83	3.5
8	271	200	3	78	0.35	2
Predicted (isotropic)					0.35	1.6
Predicted (oriented)					0.7	1.6
					n_L, Å^{-1}	R, Å
			Melt-Grown Crystals			
9	5.2	4.5	1, 3, 10		1.7, 1.2, 1.3	0, 1.9, 1.7
10	10.2	8.5	3		1.65	3
11	31	28	1, 10		1.1, 1.2	2.1, 2.5
12	97	86	3		1.55	2.6
13	271	200	3		1.3	2.6
Predicted					1.6	2

[a] The results were obtained from lines drawn through the linear portions of curves such as shown in Figures 8–14. The label material was produced by a preparative GPC by Dow Chemical Co. and kindly made available to us by Professor E. Baer (Case Western University). The matrix material was DPE of molecular weight M_w = 207 000 and M_n = 75 000. The choice of the equations to analyze the data is explained in the text. The factor of cos θ (eq 3) is 1.0 to the precision of the data. The crystallization from the melt was by cooling at 10 °C/min. The values of n_A do not take into account the oriented texture of single-crystal mats. This will increase the observed scatter in a readily calculable way, namely it will increase the intensity by a constant factor which is very nearly constant with s^2 in the experimental range, and, to within 5%, is equal to 2 for all such samples. This is assessed from the orientation of the 110 x-ray maxima which monitor the stem directions. The backgrounds from the DPE matrix are very small compared with the difference signals for all the s values shown in the figures.

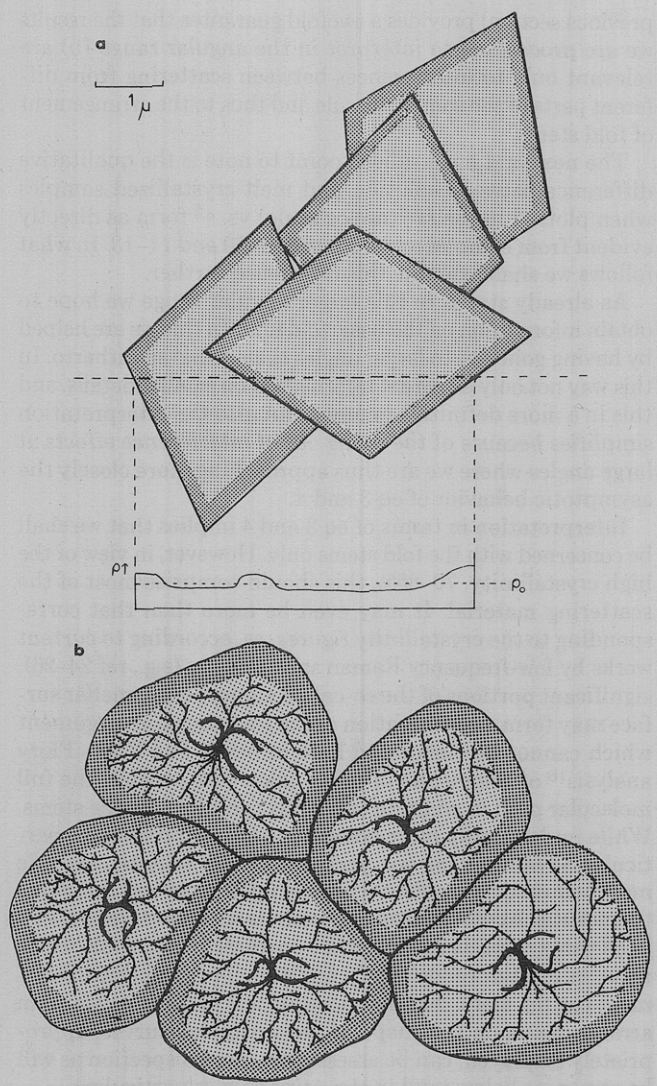

Figure 15. Schematic representation of the resulting large-scale structures for (a) solution-grown and (b) melt-grown crystals if DPE and HPE do not have exactly the same speed of crystallization. In case of (b) the zones of different DPE concentration are likely to be arranged radially as well as peripherally. As explained in the text, the resulting variations will yield intensities of the sort analyzed in Figures 4 and 6. The graph which is included in (a) illustrates variations of ρ (scattering unit density) about the average value (ρ_0) along a cross section through the crystal aggregates.

intensity attributed to the clustering in range (a) is assured; (2) to what extent does such excess intensity, if present, interfere with the interpretation of signals in range (b); and (3) with (1) and (2) assessed is there really a genuine difference between single crystals grown from solution and samples crystallized from the melt as regards adjacency or otherwise of the fold re-entry?

Angular Range (a) ($s < 0.01$ Å^{-1}). The experimental results in this angular range were plotted so as to test eq 1 (Figure 3) and 5 (Figures 4 and 6) for reasons laid out earlier. We shall take these in turn.

An analysis in terms of eq 5 could be expected to be applicable in view of the known presence of large-scale units in the structural hierarchy of a crystalline polymer, such as whole layers and layer packets in solution-crystallized, and, additionally, spherulites in the melt-crystallized material. These of course are expected to scatter at the smallest angles provided there is an associated source of contrast. Such constrast could be readily provided by the fact that HPE and DPE are thermodynamically different; the latter has a lower melting point. The situation of the crystallization of a mixture with components which differ as regards melting points but are identical in other relevant respects such as crystal structure is a familiar one. In the case of a broad molecular weight distribution, even an isotopically uniform polymer displays fractionation effects on crystallization.[8,21,22] Here, unless the polymer is cooled very rapidly, the lowest molecular weight components are ejected by the growing crystal and crystallize at a later stage forming a peripheral layer on the relevant crystal unit which thus becomes enriched in this component as schematized by Figure 15. In this way the large-scale structures become distinct not only morphologically but also as regards their molecular constitution. Now if the differing component is DPE the contrast for the relevant scattering by neutrons is provided.

It follows further that the segregation is expected to be promoted by slow crystallization and is retarded or prohibited by cross-linking as induced by radiation prior to the final crystallization (the dose in question should produce about one cross-link per molecule). Indeed this is borne out by observations (compare $(\Delta\rho)^2A$ values for samples 1 and 9 in Table II). The experience with the irradiated samples is particularly noteworthy as it suggests a method for suppressing this type of scattering contrast if such a suppression is required.

Of course the contrast requirement in itself is provided by lack of random dispersion of the DPE without the invoking of morphology as indeed envisaged previously.[13,14] However, the observation that Guinier plots do not yield straight lines in this region (Figure 3) is not readily reconciled with the notion of clusters of identifiable dimensions. The fruitfulness of the present morphological approach, however, becomes apparent by eq 5 since it is found that on plotting I^{-1} vs. s^{-4} a straight line is obtained (Figure 4). Evidence which is strongly in favor of this identification of the low-angle excess intensity is the observation (sample 19, Table I) that such signals are also observed when the structure is *known* to be of the type shown in Figure 15a. In possession of such plots the quantity $(\Delta\rho)^2A$ can be evaluated and from this A or $\Delta\rho$ provided one of them is known or assumed. The maximum possible value of $\Delta\rho$ is 0.086 D units Å^{-3} which corresponds to a weight fraction of DPE of 1 at the edges and 0 at the centers. A comparison can now be made between an estimate of A made from the neutron data and expectations of likely surface to volume ratios for the morphological units which are present in the samples. The sizes of these units are about 20 μm diameter both for solution grown aggregates of lamellae and for spherulites. Assuming complete segregation, sample 19 (Table I) gives an A value of 2.6×10^{-5} Å^{-1}, which is therefore reasonable (it should be recalled that the beam is preferentially perpendicular to the crystal lamellae). Sample 1 (Table II) gives an A value of 5×10^{-4} Å^{-1}. A sphere with such a surface to volume ratio would be of radius 0.6 μm; this is rather small, so it is quite likely that the regions of higher D concentration are not only around the spherulites (Figure 15b) but also within them. This may relate to a similar conclusion made in earlier studies on "impurity" segregation in spherulites (e.g., ref 23).

A second approach is to compare values of $(\Delta\rho)^2A$ for different samples with similar A values and hence derive an estimate of the increases in DPE concentrations at the edges of large units. For samples 12 and 19 the ratio of $(\Delta\rho)^2A$ is 1.4 to 1900. $(\Delta\rho)^2$ corresponds to contrast between the pure components for sample 19, hence the concentration difference for sample 12 is 37 times less, i.e., about 3%. For melt-grown crystals a similar exercise is possible if we assume that for slow cooling (sample 1, Table II) the fractionation is almost complete; in this way the concentration difference between zones is 2% for sample 2 in Table II. These values for $\Delta\rho$ are very

approximate, since the use of eq 5 is not at all exact, there being no compelling reason to suppose just two zones and one zone being so much larger than the other. In addition there is a degree of arbitrariness in the assumption that A is the same for the samples compared. This analysis gives no information on the size of the two zones, but it may be supposed that in the case of sample 12 the actual DPE concentrations range from 1% (say) to a maximum of 4% as compared with an average macroscopic concentration of 1.4%.

Thus the following emerges: First that we do not need to have, in fact we usually do not have, complete segregation of the isotopes, but merely enriched zones within which the distribution of the species could still be random. Second, the degree of enrichment need only be small to provide measurable contrast, which conversely means that the neutron-scattering method is rather sensitive to detect such enrichment.

Analysis by eq 1 reveals the following. We have seen that in favorable cases the initial molecular weight could be verified by neutron scattering. Even here we have excess scatter at smaller angles obeying eq 5. This implies that the tagged molecules are still molecularly dispersed although they produce scattering contrast on a larger scale. This in turn reinforces the above inferences that the DPE molecules can still be isolated entities in the enriched zone, hence the concept of enrichment, as opposed to clustering, in itself. Further, it leads to the even more general point that excess scatter at angles which are smaller than the one of interest for a particular enquiry need not necessarily interfere with the evaluation of the results at the corresponding larger angles. Specifically, in spite of the excess intensity at around $s \sim 10^{-3}$ Å^{-1}, eq 1 is still applicable at larger s. As we shall see below, the same principle applies also to successively larger angles (range (b)). This is important as it safeguards the application of the neutron-scattering technique in the appropriate angular ranges in spite of the presence of some excess intensity at low angles. Finally as regards reservations[14] about our earlier study[15] we have now verified that we can derive a physically reasonable value for I_0 on a sample used previously (No. 18, Table I) upholding the conclusion in ref 15.

Only a few comments will be made on the radius of gyration, based on the data available. In quenched melt-crystallized samples they are comparable with results from elsewhere.[14] While we have no comparison to make with the corresponding quantity in the molten state from our own work, we can usefully compare these figures with those obtained on solution-grown crystals. We note that R_g is smaller in the latter. This to our knowledge is the first instance of an R_g which has been affected by crystallization in the direction anticipated if the chains were to collapse on themselves by folding up into layers (see below). We believe this is significant. A more quantitative interpretation would need to account for the fact that the solution-crystallized samples are not isotropic and would have to allow for particular textures involved.

Angular Range (b) ($s > 0.01$ Å^{-1}). The first effect to comment on is the finding that the normalized intensities are independent of the concentration of the minority species (DPE in Figure 7 and HPE in Figures 8, 9, 11, and 12). This holds both for solution (Figures 7, 8, and 9) and melt crystallization (Figures 11 and 12). In the first place this is a very convincing test for self-consistency. For example, it verifies that the method of background subtraction is well founded. Further, it is a demonstration that the state of dispersion is independent of concentration, which implies that the local dispersion is random, since, even other evidence apart, it would be difficult to visualize a multimolecular aggregation which displays such insensitivity to concentration. This, together with the cases where the molecular weight could be directly identified by neutron scattering (in region (a), see previous section) provides a twofold guarantee that the results we are proceeding to interpret in the angular range (b) are relevant only to interferences between scattering from different parts of the same molecule and thus to the arrangement of fold stems.

The next and most salient point to note is the qualitative difference between solution and melt-crystallized samples when plotted in the Is^2 (on log scale) vs. s^2 form as directly evident from comparison of Figures 8–10 and 11–13. In what follows we shall examine this difference further.

As already stated in this larger angular range we hope to obtain information on the basic fold unit. In this we are helped by having gone out to larger angles than achieved hitherto. In this way not only do we get information on smaller details, and this in a more definitive manner, but also the interpretation simplifies because of the dying out of interference effects at large angles where we are thus approaching more closely the asymptotic behavior of eq 3 and 4.

Interpretation in terms of eq 3 and 4 implies that we shall be concerned with the fold stems only. However, in view of the high crystallinity, 70–85%, this should comprise most of the scattering material. It may even be more than that corresponding to the crystallinity figures, as, according to current works by low-frequency Raman spectroscopy (e.g., ref 24–26), significant portions of the so-called amorphous lamellar surface may form a continuation of the fold stems, an argument which cannot be elaborated here in brief. The Yoon–Flory analysis[16] of the results in ref 14 takes into account the full molecular path in addition to what is contained by the stems. While undoubtedly more complete, this would have no particular advantage for our purpose, as this requires specific model constructions about the chain paths beyond the stems themselves. As will be seen our analysis will converge to theirs in all those respects in which they are directly amenable to our tests, at least in range (b). In addition, our simplified treatment has the merit that the consequences of the relevant stem arrangements on the shape of the scattering curves, appropriately displayed, can be assessed by mere inspection as will be apparent below (and in the Appendix in particular).

When facing up to such a large number of data as in our case we shall adopt the expediency of first selecting experimental results which are simplest to interpret by eq 3 and 4 and then passing on to the more complex cases utilizing the conclusions already reached in what we consider are closer approximations to idealized models. It has proved convenient to take the melt-crystallized samples first in each case.

Simple Cases. Melt-Crystallized Material. Here straight lines could be obtained by an Is vs. s^2 plot for $s^2 > 0.0015$ Å^{-2}, i.e., according to eq 4 which then directly defines n_L and R (Figure 14 and Table IV). The model predicting such a plot is that of a rod. Thus the functional dependence of the scatter is consistent with the existence of isolated fold segments, hence fold re-entry, which is effectively statistically separated from the point of view of scattering behavior. We can test further for values of n_L (density of scattering centers along a stem) and R (the radius parameter of the rod) from intercept and slope, respectively. As seen by comparison with the values of n_L and R which are known from the chemical nature and conformation of the chain stems, the agreement with expectations from the model is good, especially since n_L and R are molecular parameters. It will be seen that expectations from a double, treble, etc., stem structure are readily apparent from this mode of presentation, as it will affect both the slope and intercept. Analytically the corresponding calculation is contained by the Appendix. It is to be noted that this embodies the effects which are pertinent to the average degree of adjacency of the fold re-entry (i.e., whether in average one, two, etc., folds are adjacently re-entrant).

Solution-Grown Crystals. Here the "simple cases" were

found only in a particular intermediate molecular weight range for the minority (HPE) component, in particular for M_w = 10 000 and 31 000. The straight lines were obtainable by Is^2 vs. s^2 plots, i.e., by eq 3 (Figures 9 and 10). These lines now define the n_A and D values in eq 3 and experimental values are shown in Table IV. We recall that results for DPE matrix (Table IV) agree with those for HPE matrix (Table III). The model predicting such a plot is a sheet. Thus here the functional dependence of the scatter is consistent with fold segments lying in a row, hence with adjacent fold re-entry. We can test for n_A (the deuterium density in the sheet) and D (the sheet thickness parameter) on the basis of this model (Table IV); account is taken here of the oriented texture of the samples. There is an agreement with experiment, in this case within a factor of 2. It will only be stated, without further elaboration, that a more perfect fit should be obtainable by modification of the sheet geometry without affecting the principal issues, i.e., the existence of sheets and the predominant adjacency of the tagged fold stems.

Other Cases. Melt-Crystallized Material. As seen from Figure 14 we have some departures from the straight line in the Is vs. s^2 plots for $s^2 > 0.0015$ Å^{-2}, the amount of the departure increasing, even if only slightly, with molecular weight of HPE. Interference between stems is a likely explanation of these departures. Interference implies non-random distribution within one molecule. A model which includes some interference between scattering from different stems would be the grouping of stems into short rows of two or more. Monodisperse populations of such groups are not consistent with the results (see above); in the Appendix the case is considered of a distribution of group sizes. It is concluded that this possibility is not likely to predict the departures from linearity as shown in Figure 14. A further possibility would be a looser grouping of the stems, such as would be provided if the chain trajectory formed a two-dimensional random walk within the crystal layer. A further discussion of this will be given elsewhere.

Solution-Grown Crystals. Most of the discussion here relates to growth at 70 °C rather than 78 °C. Departures from predictions from the simplest models occur for low molecular weights (M_w = 5000, D is measured to be 0). Other departures are for molecular weights larger than M_w = 31 000 and growth at 70 °C; in these cases D is too large (Table IV). The former is likely to be due to the fact that the chain is not long enough to form a well-defined ribbon by folding. For the high molecular weight case we invoke interference effects, between ribbons. This is more likely to arise with very long chains where different parts of a given chain may give rise to separate ribbons which would then be in close proximity, thus capable of producing interference. In this case the model for the scattering would be one dimensional, with the folded ribbons from the central parts of the molecule being relatively densely packed. A particular case of interference would be pairs of adjacent ribbons. This would increase n_A by 2 and would increase D from 1.6 to 2.7 Å. This is indeed the kind of result which is observed (Table IV) for high molecular weight and growth at 70 °C. In the case of single crystals we have corroboration (Table III) of the interference effect between ribbons from samples on which measurements in range (a) have also been made (Table I). If the folded ribbons from the same molecule can be quite closely packed laterally, we may expect a small value of R_g, which would increase slowly with molecular weight. Indeed, the results which are available show a small value of R_g, compared with the values expected for the molten state;[12] a measure of the full molecular weight dependence of R_g is an aim of further work.

In conclusion, the basic subunits are found to be rods corresponding to statistically random re-entry and sheets corresponding to adjacent re-entry for melt- and solution-crystallized samples, respectively. These conclusions represent the simplest cases; variants to it need to be hypothesized in order to account for the full range of molecular weight effects which are observed.

General Implications and Conclusions

The first principal outcome of the present work is the reassertion of the previous claim[15] that in solution-grown single crystals neutron-scattering results are consistent with the model of chains folding into layers in an adjacently reentrant manner, but this time with safeguards against the possibility of extraneous influences which have been raised in connection with it.[14] The second important result is the contrasting behavior displayed by melt-crystallized samples in which the chain stems scatter as individual entities; this would conform to random fold re-entry (see also ref 16) which we are here in a position to place in justaposition with the solution-grown crystals. Also, here this result is now established by measurements extending to large angles.

We do not intend to make further reaching generalizations based on these results which probably represent two extremes in a spectrum of behavior awaiting further exploration. We only mention that other methods exist (reviewed in ref 27) which are invoked in connection with questions of adjacency of folding, in particular a special IR technique.[28,29] Interpretations based on the IR technique are in agreement with the present conclusions concerning solution-grown crystals, but in apparent disagreement in the case of melt-grown crystals. Much of the other evidence quoted in favor of greater regularity of folding in melt-grown crystals refers to isothermal crystallization at low supercooling, e.g., as used for most morphological work and for analysis of growth kinetics. The neutron-scattering results on polyethylene do not at the moment relate to the case of low supercoolings.

In addition to the above principal points the present work provides new information on the segregation of isotopes. It demonstrates that no complete segregation, merely enrichment, needs to be involved; the neutron-scattering method is particularly sensitive to such segregation. This enrichment is associated with the large-scale morphology.

Finally, it is hoped that the present studies have helped to circumscribe conditions under which the neutron-scattering technique in question is applicable in particular angular ranges, and thus allay some fears that segregation phenomena, when they occur, provide an insuperable hinderance to the interpretation of data. It is being shown that provided due circumspection is exercised this need not be the case and in addition a method (preirradiation) by which segregation can be suppressed is also introduced.

Appendix

The main purpose of this short Appendix is to present a relatively simple method of calculation which can be used in the range $0.01 < s < 0.1$ Å^{-1} where $l > 1/s$ for many of the types of structural models under consideration. The scattering for a single stem (I_{st}) is calculated from eq 4; interference between different stems can then be calculated by multiplying I_{st} by a term which is dependent on the spacial arrangement of the stems. The examples which are illustrated involve straight rows of stems, but other models, such as a two-dimensional walk of stems (see text), could be treated.

The method is based on an equivalent equation to the usual Debye equation:

$$\text{intensity} = \sum_{i=1}^{N} \sum_{j=1}^{N} f_i f_j \frac{\sin(2\pi s r_{ij})}{2\pi s r_{ij}}$$

where f is the scattering length, r_{ij} is the distance between the

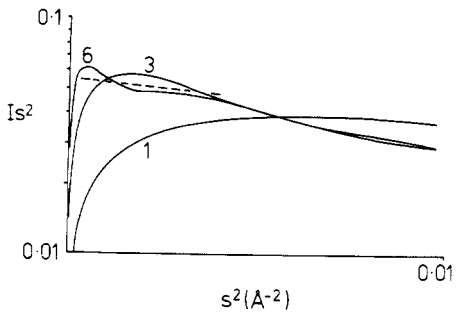

Figure 16. Calculated intensities (Appendix) for single stems and for rows of 3 and 6 stems, plotted on a similar scale to the experimental results.

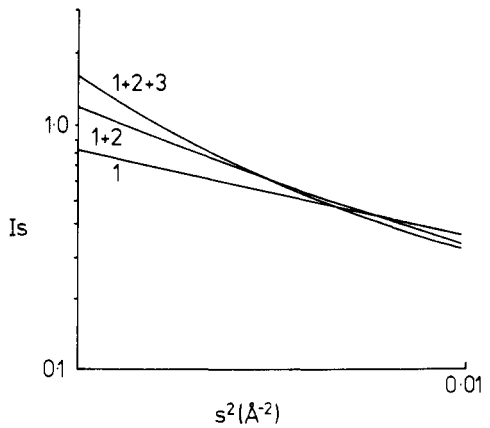

Figure 17. Calculated intensities (Appendix) for a mixed population of short rows of stems. 1 + 2 refers to equal scattering mass being in the form of single and double stems, 1 + 2 + 3 refers to single double and treble stems.

ith and the jth scatterer, and N is the number of scatterers. For a two-dimensional array of identical stems, f_i and f_j can be replaced by the intensity I_{st}. As a result of averaging in two dimensions over all possible angles between the vectors s and r_{ij} we now have for the normalized intensity

$$I = I_{st}\left\{\sum_{i=1}^{N}\sum_{j=1}^{N} J_0(2\pi r_{ij}s)\right\}/N$$

Figure 16 shows the calculated intensities for rows of 1, 3, and 6 stems. This shows that the asymptotic limit of Is^2 for very long rows (for a sheet, broken line) is approached even for quite short rows (of length about 25 Å).

We will make use of these calculations to illustrate that an interference term of the type provided by short rows of stems is not sufficient to explain the departures from linearity (predicted from the single rod model) as shown in Figure 14. Figure 17 shows calculated values of Is for a mixed population of rows 1, 2, and 3 stems. This shows not only an increase in the intercept, but also a degree of linearity, departures from which might be difficult to measure. This is not at all the observed result (Figure 14) where the departures take the form of an increase in Is above the asymptotic straight line as s^2 decreases below a value of 0.0015 Å^{-2}. A mixed population of straight rows would only be likely to predict this if it consists of single stems in addition to a small number of long rows. This would represent an ad hoc model; another type of two-dimensional arrangement seems more probable, such as a two-dimensional random walk. An analytic calculation analogous to that used for a three-dimensional coil[30] is not straightforward and is not pursued here.

Acknowledgments. We would like to express our gratitude to the staff of the Institute Laue Langevin (Grenoble), and in particular to Dr. J. Higgins, for enabling scattering measurements to be made. We also thank Dr. J. Stejny for help with GPC measurements and Mrs. A. Halter for efficient technical assistance.

References and Notes

(1) R. G. Kirste, W. A. Kruse, and J. Schelten, *Makromol. Chem.*, **162**, 299 (1973).
(2) D. G. H. Ballard, G. D. Wignall, and J. Schelten, *Eur. Polym. J.*, **9**, 965 (1973).
(3) J. P. Cotton, D. Decker, H. Benoit, B. Farnoux, J. Higgins, G. Jannink, R. Ober, C. Picot, and J. des Cloizeaux, *Macromolecules*, **7**, 863 (1974).
(4) M. Daoud, J. P. Cotton, B. Farnoux, G. Jannink, G. Sarma, H. Benoit, R. Duplessix, C. Picot, and P. G. de Gennes, *Macromolecules*, **8**, 804 (1975).
(5) A. Keller, *Rep. Prog. Phys.*, **31**, 623 (1968).
(6) B. Wunderlich, "Macromolecular Physics", Vol. I and II, Academic Press, New York, N.Y., 1973 and 1976.
(7) G. Kanig, *Kolloid Z. Z. Polym.*, **251**, 782 (1973).
(8) J. Dlugosz, G. V. Fraser, D. Grubb, A. Keller, J. A. Odell, and P. L. Goggin, *Polymer*, **17**, 471 (1976).
(9) P. J. Hendra, H. P. Jobic, and K. Holland-Moritz, *J. Polym. Sci., Polym. Lett. Ed.*, **13**, 365 (1975).
(10) P. H. Geil and J. Jones, private communication.
(11) A. H. Windle, *J. Mater. Sci.*, **10**, 252 (1975).
(12) J. Schelten, G. D. Wignall, and D. G. H. Ballard, *Polymer*, **15**, 682 (1974).
(13) J. Schelten, G. D. Wignall, D. G. H. Ballard, and W. Schmatz, *Colloid Polym. Sci.*, **252**, 749 (1974).
(14) J. Schelten, D. G. H. Ballard, G. D. Wignall, G. Longman, and W. Schmatz, *Polymer*, **17**, 751 (1976).
(15) D. M. Sadler and A. Keller, *Polymer*, **17**, 37 (1976).
(16) D. Y. Yoon and P. J. Flory, *Polymer*, **18**, 509 (1977).
(17) W. Schmatz, T. Springer, J. Schelten, and K. Ibel, *J. Appl. Crystallogr.*, **7**, 96 (1974).
(18) B. C. G. Haywood and D. L. Worcester, *J. Phys. E*, **6**, 568 (1973).
(19) A. Guinier and G. Fournet, "Small Angle Scattering of X-rays", Chapman and Hall, London, 1955.
(20) D. M. Sadler, Gordon Conference on Polymer Physics, 1976.
(21) D. M. Sadler, *J. Polym. Sci., Part A-2*, **9**, 779 (1971).
(22) A. Mehta and B. Wunderlich, *Colloid Polym. Sci.*, **253**, 193 (1975).
(23) H. D. Keith and F. J. Padden, *J. Appl. Phys.*, **35**, 1270 (1964).
(24) H. G. Olf, A. Peterlin, and W. L. Peticolas, *J. Polym. Sci., Polym. Phys. Ed.*, **12**, 359 (1974).
(25) M. J. Folkes, A. Keller, J. Stejny, G. V. Fraser, P. J. Hendra, and P. L. Goggin, *Colloid Polym. Sci.*, **13**, 341 (1975).
(26) G. R. Strobl and R. Eckel, *Colloid Polym. Sci.*, in press.
(27) A. Keller, Symposium on "The Crystallization and Fusion of Polymers", Louvain-la-Neuve, 1976, Polymer Symposia, in press.
(28) M. I. Bank and S. Krimm, *J. Polym. Sci., Part A-2*, **7**, 1785 (1969).
(29) J. H. Ching and S. Krimm, *J. Appl. Phys.*, **46**, 4181 (1975).
(30) P. Debye, Technical Report CR637 (1945) reprinted in "Light Scattering from Dilute Polymer Solutions", D. McIntyre and F. Gormick, Ed., Gordon and Breach, New York, N.Y., 1964.